Glycans

DOI: 10.1002/anie.201407976

Tracking Surface Glycans on Live Cancer Cells with Single-Molecule Sensitivity**

Hao Jiang, Brian P. English, Rachel B. Hazan, Peng Wu, and Ben Ovryn**

Abstract: *Using a combination of metabolically labeled glycans, a bioorthogonal copper(I)-catalyzed azide–alkyne cycloaddition, and the controlled bleaching of fluorescent probes conjugated to azide- or alkyne-tagged glycans, a sufficiently low spatial density of dye-labeled glycans was achieved, enabling dynamic single-molecule tracking and super-resolution imaging of N-linked sialic acids and O-linked N-acetyl galactosamine (GalNAc) on the membrane of live cells. Analysis of the trajectories of these dye-labeled glycans in mammary cancer cells revealed constrained diffusion of both N- and O-linked glycans, which was interpreted as reflecting the mobility of the glycan rather than to be caused by transient immobilization owing to spatial inhomogeneities on the plasma membrane. Stochastic optical reconstruction microscopy (STORM) imaging revealed the structure of dynamic membrane nanotubes.*

A plethora of evidence suggests that aberrant alterations in two major types of glycans on membrane proteins, that is, the N-linked and O-linked glycans, are involved in many major human diseases.[1,2] For example, increased levels of mucin glycoproteins have been found in malignant tumors of the breast, ovaries, and pancreas, and altered sialylation has been associated with increased metastatic potential,[3] but the link between the altered dynamic behaviors of these cell-surface glycoconjugates and cancer remains obscure.

Although technical advances in glycoscience and chemistry have enabled the characterization of global changes in glycosylation patterns in isolated serum glycoproteins from human patients[4] and in model organisms (e.g., zebrafish embryos),[5] only the dynamic behavior of an ensemble of cell-surface glycosylated molecules has been characterized.[6,7] The vast majority of studies, however, still utilize labeled antibodies and lectins, which can alter the dynamic behavior of the labeled molecules and thus compromise the accurate characterization of their lateral motion.

Herein, we combine metabolic glycan labeling and a bioorthogonal copper(I)-catalyzed azide–alkyne cycloaddition (CuAAC), a quintessential click reaction,[8,9] with super-resolution single-molecule tracking to unravel the dynamics of N-linked sialic acids and O-linked GalNAc on the membrane of live cells. Using the method pioneered by Reutter and Bertozzi,[5,10,11] we hijacked glycan biosynthetic pathways to incorporate a monosaccharide functionalized with a bioorthogonal chemical tag (i.e., azide or alkyne) into cell-surface glycoconjugates. As the Bertozzi copper-free click chemistry can only be used to detect the azide-tagged glycans,[11] we have applied the super-sensitive and biocompatible CuAAC that was developed by the Wu group to introduce fluorescent probes to both the azide- and alkyne-tagged glycans in live cells.[8,9]

The essence of the experimental approach is to implement total internal reflection fluorescence microscopy (TIRFM) with short laser excitation pulses (typically 0.5 ms–200 ms) that are synchronized with the user-defined exposure time of the detector such that fast moving fluorophores are detected without blurring.[12] To assure a spatial distribution of fluorescent molecules that is low enough to minimize overlap of diffusing single molecules, we generally bleach the initially high density of fluorescent probes conjugated to cell-surface glycans. Subsequently, we are able to track single molecules and analyze the individual trajectories. A large mobile fraction of labeled glycans enables bleached regions to become repopulated with fluorescent molecules, thus providing the option of implementing repeated cycles of bleaching and tracking. Furthermore, our labeling scheme, which is based upon the use of red cyanine dyes, has also enabled us to implement a strategy for super-resolution imaging using stochastic optical reconstruction microscopy (STORM),[13] which we demonstrate in live HeLa cells with numerous "microfibrils".

We used several measures to characterize the results of our single-molecule tracking experiments. The basis for this analysis is a calculation of the square displacement of each molecule in the transverse plane during the measurement time. We then determined the mean square displacement

[*] Dr. H. Jiang,[+] Prof. P. Wu
Department of Biochemistry, Albert Einstein College of Medicine
Bronx, NY 10461 (USA)
E-mail: peng.wu@einstein.yu.edu
Prof. R. B. Hazan
Department of Pathology, Albert Einstein College of Medicine
Bronx, NY 10461 (USA)
Prof. B. Ovryn
Department of Anatomy and Structural Biology
Albert Einstein College of Medicine
Bronx, NY 10461 (USA)
E-mail: ben.ovryn@einstein.yu.edu
Dr. B. P. English[+]
Janelia Farm Research Campus
Howard Hughes Medical Institute
19700 Helix Drive, Ashburn, VA 20147 (USA)

[+] These authors contributed equally.

[**] This work was partially supported by the Human Frontiers Science Program (B.E.) and the National Institute of Health (R01GM093282 to P.W. and R01GM076293 to B.O.). We thank Prof. D. Krapf, Colorado State University, for providing his Labview based tracking and MSD and CDF analysis software and for discussions.

Supporting information for this article is available on the WWW under http://dx.doi.org/10.1002/anie.201407976.

(MSD) and the cumulative distribution function (CDF). A linear scaling of the MSD with time revealed diffusive Brownian motion, whereas a sublinear scaling of the MSD implied anomalous subdiffusion. Subdiffusion in biological systems is often associated with constrained protein diffusion in the plasma membrane[14,15] or transient immobilization.[15]

We interpreted our observations of anomalous subdiffusion of surface glycans in cancer cell lines with distinct metastatic potentials as arising from diffusion under a confining potential (see the Supporting Information).[16] This damped Brownian motion models the linear scaling of the MSD at short times and its ultimate saturation.[16–18] The CDF, which describes the probability of finding a molecule within a given radius from the origin, provides additional information to determine if the probability is governed by the Gaussian statistics of a single population of Brownian walkers[19] or if the behavior is anomalous. The unprecedented spatial and temporal resolution of the movement of surface glycans that we have achieved enabled the characterization of the variation of the CDF for N-linked sialic acids and O-linked glycans with the metastatic potential of a cell.

To label cell-surface mucin-type O-glycans and sialylated glycans with fluorescent tags, we cultured two mouse mammary carcinoma cell lines, PyMT[20] and its highly metastatic variant Met-1,[21] in medium supplemented with either peracetylated *N*-azidoacetylgalactosamine, $Ac_4GalNAz$[22] (which is metabolized and installed on mucin-type O-linked glycoproteins by the polypeptide *N*-acetyl-α-galactosaminyl transferase), or peracetylated *N*-(4-pentynoyl) mannosamine, $Ac_4ManNAl$[23] (Figure 1 A,B). In a second step, cells were reacted with either an alkyne or azide bearing Alexa Fluor in the presence of the biocompatible BTTPS/Cu^I catalyst,[9] typically for less than three minutes, enabling the fluorescent tagging of the membrane glycoconjugates. The labeling specificity was verified by confocal microscopy (Supporting Information, Figure S1). Western blots suggest that owing to our short reaction times, the probes were predominately installed into sialic acids of N-linked glycoproteins (Figure S2) and not into glycolipids (Figure S3).

To reduce the initially high spatial density, we introduced a series of controlled excitation pulses (either a brief burst of strong excitation or a series of shorter, weaker pulses) to bleach some of the molecules (Figure S5 and S6, Movies S1 and S3).

Images of N-linked sialic acid in Met-1 and PyMT cells, metabolically labeled with $Ac_4ManNAl$ and conjugated with Alexa Fluor 647 azide or Alexa 488 azide, are shown in Figure 2. The boundary of the membrane and membrane-

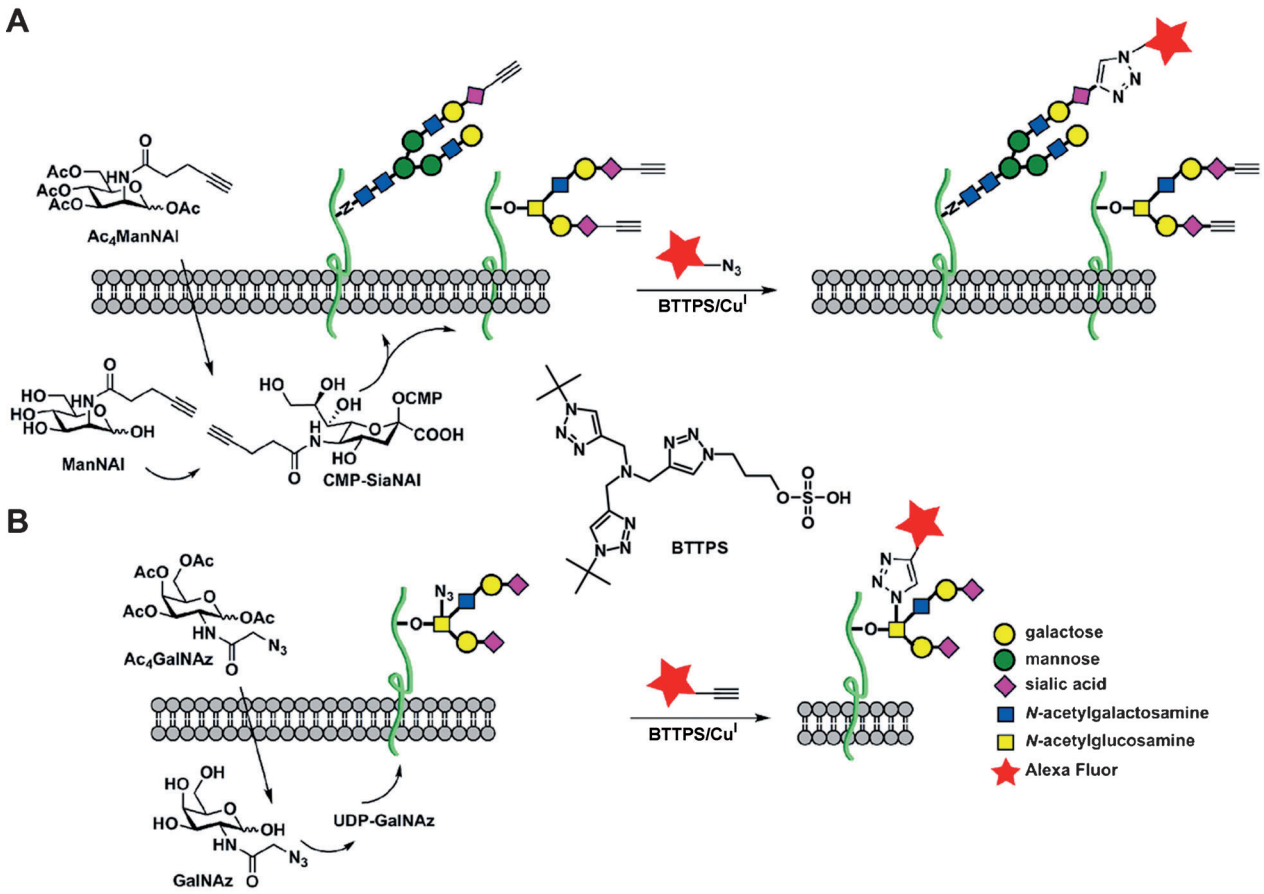

Figure 1. Imaging surface glycans using metabolic labeling and detection with CuAAC-based click chemistry. A) Metabolic labeling of sialylated glycans with $Ac_4ManNAl$ leads to the incorporation of the alkyne-bearing sialic acid (SiaNAl) into the peripheral position of both N- and O-glycans. B) Metabolic labeling of mucin-type O-glycans with $Ac_4GalNAz$ by the GalNAc salvage pathway leads to the incorporation of the azide tag into the core GalNAc. CuAAC is used to conjugate a probe to this position.

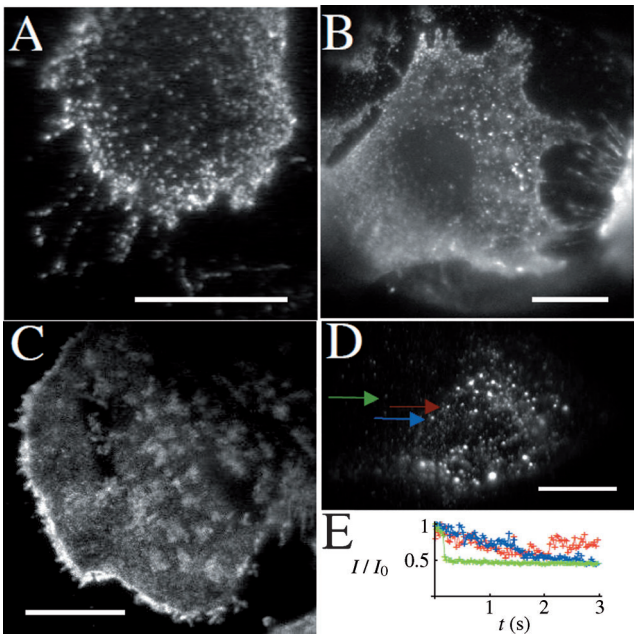

Figure 2. The imaging of sialic acid in cancer cells highlights the dynamic plasma membrane. A, B) Images of N-linked sialic acid tagged with Alexa 647 on the surface of Met-1 cells obtained after bleaching the initial majority of cell-surface molecules and excitation with 2 ms (A) and 50 ms (B) pulses (scale bars: 20 μm and 10 μm). C) PyMT cell (clicked with Alexa 488 azide) presented as a maximum projection of intensities acquired from a series of 3000 frames obtained with a 10 ms laser pulse per frame and 20 ms intervals between frames. D) Met-1 cell tagged with Alexa 647 acquired with a series of 1 ms excitation pulses spaced at 2 ms intervals; two small vesicles (red and blue) in the cell and a single molecule on the glass (green) are visible. E) Intensities of the two vesicles in (D) as a function of time after excitation with 1 ms pulses every 2 ms (red and blue); a single molecule on the glass undergoes rapid photobleaching (green). Scale bars: 20 μm (C and D).

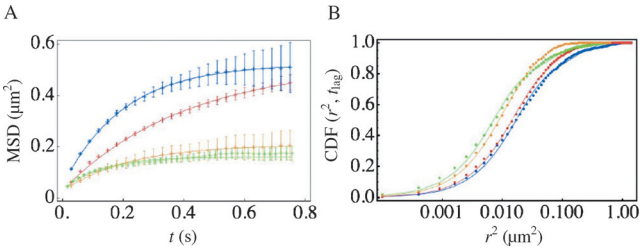

Figure 3. MSD and CDF curves for N-linked sialic acid and O-linked GalNAc glycans. A) MSD plots for the diffusion of sialic acid in PyMT and Met-1 cells (blue and red, respectively) and GalNAc in PyMT and Met-1 cells (green and orange, respectively). Fits to the MSD (——) assuming a confining harmonic potential model with the parameters given in Table 1. B) CDF for sialic acid and GalNAc in PyMT cells (blue and green, respectively) and in Met-1 cells (red and orange, respectively); fits to CDF (——) are based upon a two-component model and the values in Table 2.

tunneling nanotubes were observed;[24–26] these nanotubes are a persistent feature of metastatic cells (Movies S1–S3). The bright border region in the maximum intensity projection of Figure 2C (ca. 1.2 μm in width) is particularly pronounced. Dynamic tracking of single molecules (Movies S1 and S2) clearly indicates highly mobile glycans. By contrast, fluorescently labeled sialylated glycans can aggregate in endocytic vesicles (Figure 2D), which are relatively immobile, have a broad size distribution, and are resistant to photobleaching; indeed, we have observed that the fluorescence in a vesicle can increase (e.g., Figure 2E, red trace).

We tracked hundreds of diffusing single molecules for hundreds of frames and analyzed the individual trajectories of the cell-surface glycans. Figure 3 shows the MSD and CDF curves obtained for sialic acid in PyMT and Met-1 cells (blue and red, respectively) and GalNAc in these cell types (green and orange, respectively). Glycans appear to move freely for short time lags (Figure 3A), but the initial linear scaling saturates as they sense constrained diffusion at longer times. The slope of the linear portion of the MSD yields the probability density distribution of diffusion constants for a population of freely diffusing molecules (see Figure S7 for histograms of the probability density of the MSD for freely diffusing glycans).

We modeled the observed anomalous diffusion assuming that molecules behave as Brownian walkers that experience a frictional force with coefficient γ and are confined by a harmonic potential, $U(\mathbf{r}) = \frac{k\mathbf{r}^2}{2}$, with stiffness k (see the Supporting Information).[16–18] The best fits obtained using this model are shown in Figure 3A, and the parameters are found in Table 1; the residual errors in these fits are shown in Figure S9A.

Table 1: Spring constant and friction coefficients.

Tagged glycan (cell type)	k [μN m^{-1}]	γ [Pa s μm]
sialic acid (PyMT)	0.017	0.004
sialic acid (Met-1)	0.018	0.007
GalNAc (PyMT)	0.07	0.009
GalNAc (Met-1)	0.05	0.01

The CDFs were poorly fit by a single exponential, indicating that the diffusion is not governed by the motion of a population of molecules moving with a single diffusion coefficient (see the Supporting Information). Therefore, we fitted the data using an alternative model that is based upon two-component mobility with slow and fast components, α_1 and α_2, and diffusion constants D_1 and D_2; $\alpha_1 \approx 1$ corresponds to normal diffusion with constant D_1 (see the Supporting Information).[15,19,27] The solid lines (Figure 3B) are fits obtained with this model; the corresponding parameters are shown in Table 2 and the residual errors in these fits in Figure S9B.

Table 2: Values of α and diffusion constants.

Tagged glycan (cell type)	α	D_1 [μm^2 s^{-1}]	D_2 [μm^2 s^{-1}]
sialic acid (PyMT)	0.71	0.13	1.15
sialic acid (Met-1)	0.63	0.11	0.58
GalNAc (PyMT)	0.72	0.09	0.91
GalNAc (Met-1)	0.55	0.06	0.24

Aside from tracking the dynamics of single molecules, we were also able to superpose the images of hundreds of single molecules and obtain super-resolution images as a function of time. Furthermore, we have used our labeling scheme, which is based upon red cyanine dyes, to implement a strategy for super-resolution imaging using STORM in live cells. HeLa cells metabolically labeled with Ac_4ManNAl and conjugated with Alexa Fluor 647 azide are shown in Figure 4. A single image from a series of 480 images was obtained using a sequence of 405 nm light (10 ms) followed by excitation with 637 nm light (30 ms; Figure 4 A, see also the Supporting Information). Figure 4 B shows the corresponding STORM image produced from 130 021 detected molecules; the centroid of each is displayed by a Gaussian with a standard deviation that was determined from the localization precision. The mean localization error is 37 nm;[28] a larger version of Figure 4 B is provided in Figure S10. The STORM approach enabled the controlled super-resolution imaging of membrane structures and thin nanotubes in live cells.

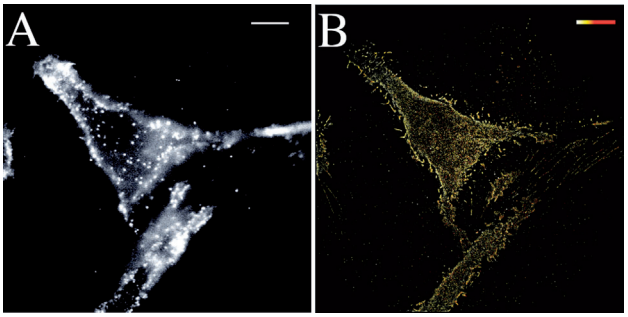

Figure 4. STORM imaging of sialic acid in HeLa cells. HeLa cells were metabolically labeled with Ac_4ManNAl and conjugated with Alexa Fluor 647 azide. A) Single STORM image (100th frame) from a sequence. B) STORM image produced from 480 consecutive frames. The 130 021 detected molecules are displayed by a Gaussian with a standard deviation equal to the localization precision. The color bar represents the integrated fluorescent intensity of each molecule. Scale bars: 10 μm.

The delineation of membrane nanotubes using either our single-molecule tracking method (Figure 2) or STORM imaging (Figure 4) has enabled the direct visualization of the dynamic movement of glycans on the surface of these fine structures. This work complements prior nanotube visualization strategies using direct membrane labeling with lipophilic dyes and indirect measurements using labels for actin and intracellular organelles.[24,25] Although lipid-containing photoswitchable probes have enabled membrane imaging with STORM,[29] and the transfer of intracellular cargo between cells along nanotubes has been observed, our live-cell imaging can track dynamic changes in nanotube morphology and the transfer of surface glycans between cells (Movies S1–S3). Furthermore, our dynamic tracking and live-cell STORM imaging, as compared to fixed-cell imaging of glycans using dSTORM,[30] can be used to directly distinguish between static clusters of glycans and mobile, diffusing glycans. Many of the features in Figure 4 B may appear suggestive of static clusters, but we are able to conclude that these represent dynamic glycans.

The application of single-molecule tracking to quantify the movement of proteins in the plasma membrane has revealed a rich behavior, including anomalous diffusion owing to confinement or immobilization.[14,15] There are two key factors, however, that contribute to the mobility of single fluorescent molecules on labeled glycans: the mobility of the glycan and the mobility of the protein. Furthermore, the movement depends upon the location of the fluorescent molecule on the particular glycan (i.e., whether the probe is in a rigid or flexible part of the glycan) and upon how the density of the glycoproteins on the cell surface affects the polymer brush. Our MSD and CDF measurements provide information that capture these complex dynamics.

The CDFs that we have measured for both sialic acid and GalNAc (in two cell types) are poorly fit with a single diffusion constant, which suggests that the motion is not normal Brownian diffusion. Instead, the CDFs are best fit by assuming a two-component mobility, which provides evidence of anomalous diffusion. As these two-component fits (Table 2) share a common slow diffusing component (ca. 0.1 $\mu m^2 s^{-1}$), but differ mainly in their fast diffusion component, we interpret the slower component as representing the lateral diffusion of the protein in the plasma membrane and the fast component as representing the diffusion of the fluorescent molecule on the glycan.

We have determined that the MSD for glycans is linear when they are observed over short times and that it reaches a saturation value over longer time periods. The linear portion is suggestive of Brownian motion, and the saturation indicates damped diffusion in a confining harmonic potential that reflects the glycan structure. Consistent with this model, the data indicate that the spring constant for N-linked sialic acid is several times weaker than for GalNAc in both cell types, suggesting that N-linked sialic acid is less constrained (Table 1).

Furthermore, the distribution of diffusion constants calculated from the linear, freely diffusing portion of the MSD (Figure S7) indicates that the diffusion is skewed towards faster values for N-linked sialic acid relative to GalNAc in both cell types. The faster motility of sialic acid may further reflect its position at the non-reducing terminal position of N-linked glycans attached by galactose by α2,3- or α2,6-linkages; compared with GalNAc, which is a core residue attached to the polypeptide backbone, sialic acid should move more freely.

Significantly, the data suggest that N-linked sialic acid diffuses more slowly (by a factor of two) in cells that have a high metastatic potential as compared to cells with a low metastatic potential, and O-linked GalNAc appears to diffuse nearly three times more slowly in Met-1 than in PyMT. We speculate that the observed slower diffusion of glycans on the surface of cells with higher metastatic potentials may reflect the increased crowding of the tethered polymers.[31–33] Currently, we are using mass spectrometry to analyze the glycan structures from the two cell lines to determine if this is specifically related to the size of the glycan structures or a possible increase in overall sialylation.[34,35]

We conjecture that there may be regions on some cell surfaces, in particular in regions with pronounced galectin binding[36] and near integrin adhesions, where local spatial averages will not yield the same result as the MSD calculated from temporal trajectories. As cell-surface glycans, which act as sensors of the extracellular matrix, are considerably longer than integrins, the formation of adhesions likely requires local glycan clearance by a combination of mechanisms, involving lateral movement, endocytosis, and shedding.[37,38] We expect such processes to have a significant impact on the movement of glycans in the vicinity of adhesions and in particular for the tracking of sialic acids on single proteins such as integrins, which have been shown to undergo constrained diffusion with diffusion constants and confinement radii that depend upon whether the integrin is within or outside of adhesions.[39]

Our data also demonstrate that the imaging of surface glycans in live cells can provide superb detail regarding the morphology of the plasma membrane. One limitation of our metabolic labeling approach coupled with bioorthogonal chemistry, however, is that all glycans on the cell surface containing the tagged monosaccharide building blocks are labeled. Accordingly, glycoforms of a specific protein target cannot be uniquely detected. To overcome this limitation, we are currently implementing a double labeling strategy that combines our glycan labeling techniques with recently developed site-specific protein labeling techniques to enable the imaging of sialylated glycans of a specific membrane protein such that we will be able to simultaneously track the movement of the protein in the membrane and the differential movement of the tethered glycan.[40]

Received: August 6, 2014
Revised: October 9, 2014
Published online: December 16, 2014

Keywords: click chemistry · glycans · membrane proteins · single-molecule studies · stochastic optical reconstruction microscopy (STORM)

[1] S. Hakomori, *Proc. Natl. Acad. Sci. USA* **2002**, *99*, 10231.
[2] "Glycosylation Changes in Cancer": A. Varki, R. Kannagi, B. P. Toole in *Essentials of glycobiology* (Eds.: A. Varki, R. D. Cummings, J. D. Esko, H. H. Freeze, P. Stanley, C. R. Bertozzi, G. W. Hart, M. E. Etzler), Cold Spring Harbor Laboratory Press, Cold Spring (NY), **2009**.
[3] L. Yang, J. O. Nyalwidhe, S. Guo, R. R. Drake, O. J. Semmes, *Mol. Cell. Proteomics* **2011**, *10*, DOI: 10.1074/mcp.M110.007294.
[4] L. R. Ruhaak, S. Miyamoto, C. B. Lebrilla, *Mol. Cell. Proteomics* **2013**, *12*, 846.
[5] S. T. Laughlin, J. M. Baskin, S. L. Amacher, C. R. Bertozzi, *Science* **2008**, *320*, 664.
[6] M. Wier, M. Edidin, *Science* **1988**, *242*, 412.
[7] M. Edidin, *Immunol. Res.* **2010**, *47*, 265.
[8] C. Besanceney-Webler, H. Jiang, T. Zheng, L. Feng, D. S. del Amo, W. Wang, L. M. Klivansky, F. L. Marlow, Y. Liu, P. Wu, *Angew. Chem. Int. Ed.* **2011**, *50*, 8051; *Angew. Chem.* **2011**, *123*, 8201.
[9] W. Wang, S. Hong, A. Tran, H. Jiang, R. Triano, Y. Liu, X. Chen, P. Wu, *Chem. Asian J.* **2011**, *6*, 2796.
[10] O. T. Keppler, R. Horstkorte, M. Pawlita, C. Schmidt, W. Reutter, *Glycobiology* **2001**, *11*, 11R.
[11] S. Laughlin, C. Bertozzi, *Proc. Natl. Acad. Sci. USA* **2009**, *106*, 12.
[12] B. P. English, V. Hauryliuk, A. Sanamrad, S. Tankov, N. H. Dekker, J. Elf, *Proc. Natl. Acad. Sci. USA* **2011**, *108*, E365.
[13] M. J. Rust, M. Bates, X. Zhuang, *Nat. Methods* **2006**, *3*, 793.
[14] S. Condamin, V. Tejedor, R. Voituriez, O. Bénichou, J. Klafter, *Proc. Natl. Acad. Sci. USA* **2008**, *105*, 5675.
[15] A. V. Weigel, B. Simon, M. M. Tamkun, D. Krapf, *Proc. Natl. Acad. Sci. USA* **2011**, *108*, 6438.
[16] J.-H. Jeon, R. Metzler, *Phys. Rev. E* **2012**, *85*, 021147.
[17] B. Lukic, S. Jeney, Z. Sviben, A. J. Kulik, E.-L. Florin, L. Forro, *Phys. Rev. E* **2007**, *76*, 011112.
[18] J.-H. Jeon, N. Leijnse, L. B. Oddershede, R. Metzler, *New J. Phys.* **2013**, *15*, 045011.
[19] G. J. Schütz, H. Schindler, T. Schmidt, *Biophys. J.* **1997**, *73*, 1073.
[20] J. Hulit, K. Suyama, S. Chung, R. Keren, G. Agiostratidou, W. Shan, X. Dong, T. M. Williams, M. P. Lisanti, K. Knudsen, R. B. Hazan, *Cancer Res.* **2007**, *67*, 3106.
[21] A. D. Borowsky, R. Namba, L. J. T. Young, K. W. Hunter, J. G. Hodgson, C. G. Tepper, E. T. McGoldrick, W. J. Muller, R. D. Cardiff, J. P. Gregg, *Clin. Exp. Metastasis* **2005**, *22*, 47.
[22] H. C. Hang, C. Yu, D. L. Kato, C. R. Bertozzi, *Proc. Natl. Acad. Sci. USA* **2003**, *100*, 14846.
[23] P. V. Chang, X. Chen, C. Smyrniotis, A. Xenakis, T. Hu, C. R. Bertozzi, P. Wu, *Angew. Chem. Int. Ed.* **2009**, *48*, 4030; *Angew. Chem.* **2009**, *121*, 4090.
[24] X. Wang, M. L. Veruki, N. V. Bukoreshtliev, E. Hartveit, H.-H. Gerdes, *Proc. Natl. Acad. Sci. USA* **2010**, *107*, 17194.
[25] A. Chauveau, A. Aucher, P. Eissmann, E. Vivier, D. M. Davis, *Proc. Natl. Acad. Sci. USA* **2010**, *107*, 5545.
[26] E. Lou, S. Fujisawa, A. Barlas, Y. Romin, K. Manova-Todorova, M. A. S. Moore, S. Subramanian, *Commun. Integr. Biol.* **2012**, *5*, 399.
[27] S. J. Sahl, M. Leutenegger, M. Hilbert, S. W. Hell, C. Eggeling, *Proc. Natl. Acad. Sci. USA* **2010**, *107*, 6829.
[28] K. I. Mortensen, L. S. Churchman, J. A. Spudich, H. Flyvbjerg, *Nat. Methods* **2010**, *7*, 377.
[29] S. H. Shim, C. Xia, G. Zhong, H. P. Babcock, J. C. Vaughan, B. Huang, X. Wang, C. Xu, G. Q. Bi, X. Zhuang, *Proc. Natl. Acad. Sci. USA* **2012**, *109*, 13978.
[30] S. Letschert, A. Ghler, C. Franke, N. Bertleff-Zieschang, E. Memmel, S. Doose, J. Seibel, M. Sauer, *Angew. Chem. Int. Ed.* **2014**, *53*, 10921; *Angew. Chem.* **2014**, *126*, 11101.
[31] M. Edidin, S. C. Kuo, M. P. Sheetz, *Science* **1991**, *254*, 1379.
[32] M. P. Sheetz, *Annu. Rev. Biophys. Biomol. Struct.* **1993**, *22*, 417.
[33] M. A. Deverall, E. Gindl, E.-K. Sinner, H. Besir, J. Ruehe, M. J. Saxton, C. A. Naumann, *Biophys. J.* **2005**, *88*, 1875.
[34] D. Dube, C. Bertozzi, *Nat. Rev. Drug Discovery* **2005**, *4*, 477.
[35] S. Iyer, R. M. Gaikwad, V. Subba-Rao, C. D. Woodworth, I. Sokolov, *Nat. Nanotechnol.* **2009**, *4*, 389.
[36] K. S. Lau, E. A. Partridge, A. Grigorian, C. I. Silvescu, V. N. Reinhold, M. Demetriou, J. W. Dennis, *Cell* **2007**, *129*, 123.
[37] J. A. Roper, R. C. Williamson, M. D. Bass, *Curr. Opin. Struct. Biol.* **2012**, *22*, 583.
[38] E. Atilgan, B. Ovryn, *Biophys. J.* **2009**, *96*, 3555.
[39] O. Rossier, V. Octeau, J.-B. Sibarita, C. Leduc, B. Tessier, D. Nair, V. Gatterdam, O. Destaing, C. Albiges-Rizo, R. Tampe, L. Cognet, D. Choquet, B. Lounis, G. Giannone, *Nat. Cell Biol.* **2012**, *14*, 1057.
[40] I. Chen, A. Y. Ting, *Curr. Opin. Biotechnol.* **2005**, *16*, 35.

